

Investigation of the $dd \rightarrow {}^3\text{He}\pi^0$ reaction with the FZ Jülich WASA-at-COSY facility

P. Adlarson,¹ W. Augustyniak,² W. Bardan,³ M. Bashkanov,^{4,5} F.S. Bergmann,⁶ M. Berłowski,⁷ H. Bhatt,⁸ M. Büscher,^{9,10} H. Calén,¹ I. Ciepał,³ H. Clement,^{4,5} D. Coderre,^{9,10,11} E. Czerwiński,³ K. Demmich,⁶ E. Doroshkevich,^{4,5} R. Engels,^{9,10} W. Erven,^{12,10} W. Eyrich,¹³ P. Fedorets,^{9,10,14} K. Föhl,¹⁵ K. Fransson,¹ F. Goldenbaum,^{9,10} P. Goslawski,⁶ A. Goswami,¹⁶ K. Grigoryev,^{9,10,17} C.–O. Gullström,¹ C. Hanhart,^{9,10,18} F. Hauenstein,¹³ L. Heijkskjöld,¹ V. Hejny,^{9,10,*} F. Hinterberger,¹⁹ M. Hodana,^{3,9,10} B. Höistad,¹ A. Jany,³ B.R. Jany,³ L. Jarczyk,³ T. Johansson,¹ B. Kamys,³ G. Kemmerling,^{12,10} F.A. Khan,^{9,10} A. Khoukaz,⁶ D.A. Kirillov,²⁰ S. Kistryn,³ J. Klaja,³ H. Kleines,^{12,10} B. Kłos,²¹ M. Krapp,¹³ W. Krzemień,³ P. Kulesa,²² A. Kupść,^{1,7} K. Lalwani,^{8,†} D. Lersch,^{9,10} L. Li,¹³ B. Lorentz,^{9,10} A. Magiera,³ R. Maier,^{9,10} P. Marciniowski,¹ B. Mariański,² M. Mikirtychians,^{9,10,11,17} H.–P. Morsch,² P. Moskal,³ B.K. Nandi,⁸ H. Ohm,^{9,10} I. Ozerianska,³ E. Perez del Rio,^{4,5} N.M. Piskunov,²⁰ P. Pluciński,^{1,‡} P. Podkopał,^{3,9,10} D. Prasuhn,^{9,10} A. Pricking,^{4,5} D. Pszczel,^{1,7} K. Pysz,²² A. Pysznik,^{1,3} C.F. Redmer,^{1,§} J. Ritman,^{9,10,11} A. Roy,¹⁶ Z. Rudy,³ S. Sawant,⁸ A. Schmidt,¹³ S. Schadmand,^{9,10} T. Seifick,^{9,10} V. Serdyuk,^{9,10,23} N. Shah,^{8,¶} M. Siemaszko,²¹ R. Siudak,²² T. Skorodko,^{4,5} M. Skurzok,³ J. Smyrski,³ V. Sopot,¹⁴ R. Stassen,^{9,10} J. Stepaniak,⁷ E. Stephan,²¹ G. Sterzenbach,^{9,10} H. Stockhorst,^{9,10} H. Ströher,^{9,10} A. Szczurek,²² T. Tolba,^{9,10,**} A. Trzciński,² R. Varma,⁸ G.J. Wagner,^{4,5} W. Węglorz,²¹ M. Wolke,¹ A. Wrońska,³ P. Wüstner,^{12,10} P. Wurm,^{9,10} A. Yamamoto,²⁴ X. Yuan,²⁵ J. Zabierowski,²⁶ C. Zheng,²⁵ M.J. Zieliński,³ W. Zipper,²¹ J. Złomańczuk,¹ P. Żuprański,² and M. Żurek³

(WASA-at-COSY Collaboration)

¹Division of Nuclear Physics, Department of Physics and Astronomy, Uppsala University, Box 516, 75120 Uppsala, Sweden²Department of Nuclear Physics, National Centre for Nuclear Research, ul. Hoza 69, 00-681, Warsaw, Poland³Institute of Physics, Jagiellonian University, ul. Reymonta 4, 30-059 Kraków, Poland⁴Physikalisches Institut, Eberhard–Karls–Universität Tübingen, Auf der Morgenstelle 14, 72076 Tübingen, Germany⁵Kepler Center for Astro and Particle Physics, Eberhard Karls

University Tübingen, Auf der Morgenstelle 14, 72076 Tübingen, Germany

⁶Institut für Kernphysik, Westfälische Wilhelms–Universität Münster, Wilhelm–Klemm–Str. 9, 48149 Münster, Germany⁷High Energy Physics Department, National Centre for Nuclear Research, ul. Hoza 69, 00-681, Warsaw, Poland⁸Department of Physics, Indian Institute of Technology Bombay, Powai, Mumbai–400076, Maharashtra, India⁹Institut für Kernphysik, Forschungszentrum Jülich, 52425 Jülich, Germany¹⁰Jülich Center for Hadron Physics, Forschungszentrum Jülich, 52425 Jülich, Germany¹¹Institut für Experimentalphysik I, Ruhr–Universität Bochum, Universitätsstr. 150, 44780 Bochum, Germany¹²Zentralinstitut für Engineering, Elektronik und Analytik, Forschungszentrum Jülich, 52425 Jülich, Germany¹³Physikalisches Institut, Friedrich–Alexander–Universität

Erlangen–Nürnberg, Erwin–Rommel–Str. 1, 91058 Erlangen, Germany

¹⁴Institute for Theoretical and Experimental Physics, State Scientific Center of

the Russian Federation, Bolshaya Chermushkinskaya 25, 117218 Moscow, Russia

¹⁵II. Physikalisches Institut, Justus–Liebig–Universität Gießen, Heinrich–Buff–Ring 16, 35392 Giessen, Germany¹⁶Department of Physics, Indian Institute of Technology Indore, Khandwa Road, Indore–452017, Madhya Pradesh, India¹⁷High Energy Physics Division, Petersburg Nuclear Physics Institute,

Orlova Roshka 2, Gatchina, Leningrad district 188300, Russia

¹⁸Institute for Advanced Simulation, Forschungszentrum Jülich, 52425 Jülich, Germany¹⁹Helmholtz–Institut für Strahlen– und Kernphysik, Rheinische

Friedrich–Wilhelms–Universität Bonn, Nußallee 14–16, 53115 Bonn, Germany

²⁰Veksler and Baldin Laboratory of High Energy Physics, Joint Institute

for Nuclear Physics, Joliot–Curie 6, 141980 Dubna, Moscow region, Russia

²¹August Chelkowski Institute of Physics, University of Silesia, Uniwersytecka 4, 40-007, Katowice, Poland²²The Henryk Niewodniczański Institute of Nuclear Physics, Polish

Academy of Sciences, 152 Radzikowskiego St, 31-342 Kraków, Poland

²³Dzhelepov Laboratory of Nuclear Problems, Joint Institute for Nuclear

Physics, Joliot–Curie 6, 141980 Dubna, Moscow region, Russia

²⁴High Energy Accelerator Research Organisation KEK, Tsukuba, Ibaraki 305–0801, Japan²⁵Institute of Modern Physics, Chinese Academy of Sciences, 509 Nanchang Rd., Lanzhou 730000, China²⁶Department of Cosmic Ray Physics, National Centre for Nuclear Research, ul. Uniwersytecka 5, 90–950 Łódź, Poland

(Dated: July 22, 2013)

An exclusive measurement of the $dd \rightarrow {}^3\text{He}\pi^0$ reaction was carried out at a beam momentum of $p_a = 1.2$ GeV/c using the WASA-at-COSY facility. Information on the total cross section as well as differential distributions was obtained. The data are described by a phenomenological approach based on a combination of a quasi-free model and a partial wave expansion for the three-body

reaction. The total cross section is found to be $\sigma_{tot} = (2.89 \pm 0.01_{stat} \pm 0.06_{sys} \pm 0.29_{norm}) \mu b$. The contribution of the quasi-free processes (with the beam or target neutron being a spectator) accounts for 38% of the total cross section and dominates the differential distributions in specific regions of phase space. The remaining part of the cross section can be described by a partial wave decomposition indicating the significance of p -wave contributions in the final state.

PACS numbers: 13.75.-n, 21.45.-v, 25.10.+s, 25.45.-z

Keywords: deuteron-deuteron interaction, pion production, few nucleon system

INTRODUCTION

At the fundamental level of the Standard Model, isospin violation is due to quark mass differences as well as electromagnetic effects [1–3]. Therefore, the observation of isospin violation is an experimental tool to study quark mass effects in hadronic processes. However, in general isospin violating observables are largely dominated by the pion mass differences, which are enhanced due to the small pion mass. An exception are charge symmetry breaking (CSB) observables. Charge symmetry is the invariance of a system under rotation by 180° around the second axis in isospin space that interchanges up and down quarks. It transforms a π^+ into a π^- and, therefore, the pion mass difference does not contribute. Ref. [4] calls the investigation of CSB effects one of the most challenging subjects in hadron physics. On the basis of theoretical approaches with a direct connection to QCD, like lattice QCD or effective field theory, it is possible to study quark mass effects on the hadronic level, since the effects of virtual photons are under control — for a detailed discussion on this subject see Ref. [5].

The first observation of the charge symmetry breaking $dd \rightarrow {}^4\text{He}\pi^0$ reaction was reported for beam energies very close to the reaction threshold [6]. At the same time information on CSB in $np \rightarrow d\pi^0$ manifesting itself in a forward-backward asymmetry became available [7]. These data triggered advanced theoretical calculations within effective field theory, providing the opportunity to investigate the influence of the quark masses in nuclear physics [8, 9]. This is done using Chiral Perturbation Theory (ChPT) which has been extended to pion production reactions [10]. First steps towards a theoretical understanding of the $dd \rightarrow {}^4\text{He}\pi^0$ reaction have been taken [11, 12]. Soft photon exchange in the initial state could significantly enhance the cross section for $dd \rightarrow {}^4\text{He}\pi^0$ [13]. However, it was demonstrated in Ref. [14] that a simultaneous analysis of CSB in the two-nucleon sector and in $dd \rightarrow {}^4\text{He}\pi^0$ strongly constrains the calculations.

The main problem in the calculation of $dd \rightarrow {}^4\text{He}\pi^0$ is to get theoretical control over the isospin symmetric part of the initial state interactions, for here high accuracy wave functions are needed for $dd \rightarrow 4N$ in low partial waves at relatively high energies. These can be accessed by measurements of other, isospin conserving, dd induced pion production reaction channels at a similar excess en-

ergy, such that the final state (and, thus, also the initial state) is constrained to small angular momenta. Then, the incoming system shares some of the partial waves in the initial state with the reaction $dd \rightarrow {}^4\text{He}\pi^0$, while the transition operator is calculable with sufficient accuracy using ChPT. Such a reaction is $dd \rightarrow {}^3\text{He}n\pi^0$ and the corresponding measurement is presented here.

EXPERIMENT

The experiment was carried out at the Institute for Nuclear Physics of Forschungszentrum Jülich in Germany using the Cooler Synchrotron COSY [15] together with the WASA detection system. For the measurement of $dd \rightarrow {}^3\text{He}n\pi^0$ at an excess energy of $Q \approx 40$ MeV a deuteron beam with a momentum of 1.2 GeV/c was scattered on frozen deuterium pellets provided by an internal pellet target. The reaction products ${}^3\text{He}$ and π^0 were detected by the Forward Detector and the Central Detector of the WASA facility, respectively, while the neutron remained undetected. The Forward Detector consists of several layers of plastic scintillators for particle identification and energy reconstruction and an array of straw tubes for precise tracking. The polar angular range between 3° and 18° fully covers the angular range of the outgoing ${}^3\text{He}$ with the exception of very small angles. At this beam momentum the ${}^3\text{He}$ ejectiles have kinetic energies in the range of 65 - 214 MeV and, thus, are already stopped in the first detector layers: in addition to the straw tube tracker only the two 3 mm thick layers of the Forward Window Counter and the first 5 mm thick layer of the Forward Trigger Hodoscope were used. The two photons from the π^0 decay were detected by the Scintillator Electromagnetic Calorimeter as part of the Central Detector. Photons were distinguished from charged particles using the Plastic Scintillator Barrel located inside the calorimeter. The experiment trigger was based on a coincidence between a high energy deposit in both layers of the Forward Window Counter together with a veto condition on the first layer of the Forward Range Hodoscope to select helium ejectiles and a low energy neutral cluster ($E > 20$ MeV) in the calorimeter to tag the decay of the pion. Further information on the WASA-at-COSY facility can be found in Ref.[16].

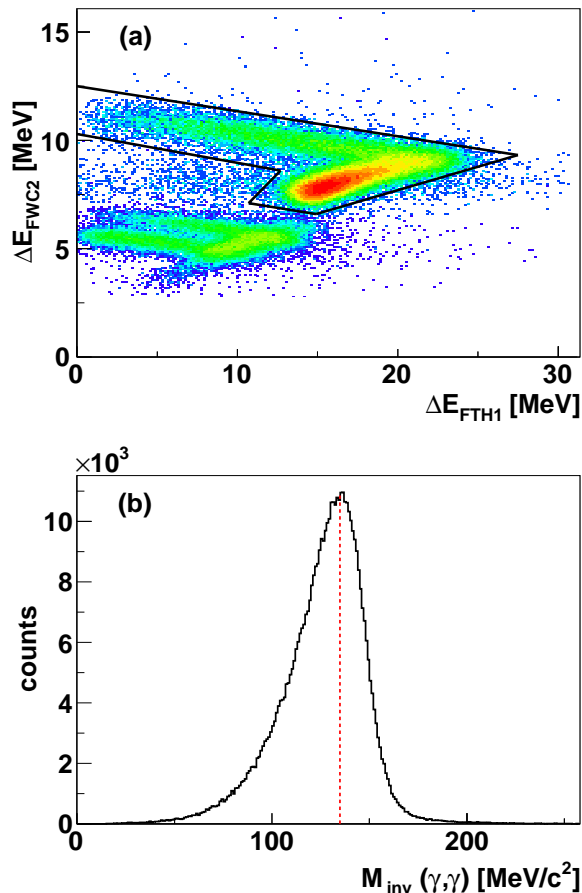


FIG. 1. (Color online) (a) Energy loss in the Forward Window Counter versus energy loss in the first layer of the Forward Trigger Hodoscope. The obtained energy pattern shows a clear separation between different particles types. The graphical cut indicated in black represents the region used to select ${}^3\text{He}$ candidates. (b) The two photon invariant mass distribution corresponding to the $\pi^0 \rightarrow \gamma\gamma$ decay. The red dotted line indicates the π^0 mass.

DATA ANALYSIS

Apart from the charge symmetry breaking reaction $dd \rightarrow {}^4\text{He}\pi^0$ with a four orders of magnitude smaller cross section, $dd \rightarrow {}^3\text{He}n\pi^0$ is the only process with a charge 2 particle and a neutral pion in final state. Thus, the identification of a forward going helium and two neutral tracks forming a pion already provides a clean signature for this reaction. Helium isotopes are identified by means of $\Delta E - \Delta E$ plots using the energy deposit in the Forward Window Counter and the first layer of the Forward Trigger Hodoscope (Fig. 1a).

The condition that the ${}^3\text{He}$ has to pass at least the first two scintillator layers introduces an additional acceptance cut of $E_{\text{kin}} > 125$ MeV. This rejects most of the ${}^3\text{He}$ going backward in the c.m. system. However, having two

identical particles in the initial state and, thus, a symmetric angular distribution with respect to $\theta_{\text{c.m.}} = 90^\circ$ the full angular range can be recovered by a symmetrization of the detected events. The energy deposits are also used to reconstruct the ${}^3\text{He}$ kinetic energy by matching the energy loss pattern to Monte-Carlo simulations. The ${}^3\text{He}$ four-momentum is completed by the direction information from the straw tube tracker. In addition to the ${}^3\text{He}$ two neutral clusters in the central detector corresponding to the two photons from the π^0 decay were requested. As event pile-up and low energy satellites of genuine photon clusters can cause larger photon multiplicities the most probable true two-photon combination was identified by selecting the pair with the ${}^3\text{He} - \pi^0$ missing mass being closest to the neutron mass. As result a nearly background free pion peak was obtained (Fig. 1b). In a final step the data were refined by applying a kinematic fit using the hypothesis $dd \rightarrow {}^3\text{He}n\pi^0$. Still remaining background and badly reconstructed events were rejected by a cut on the cumulated probability distribution at 10%. At the end of the analysis chain about 3.4×10^6 fully reconstructed and background free $dd \rightarrow {}^3\text{He}n\pi^0$ events are available. Although based on this data set any possible differential distribution can be generated — e.g. for a selective comparison with future microscopic theoretical calculations — a suitable set of observables for further analysis and presentation had to be selected. For any unpolarized measurement with three particles in final state four independent variables fully describe the reaction kinematics. For the present analysis the choice for these independent variables is based on the Jacobi momenta \vec{q} and \vec{p} with \vec{q} being the π^0 momentum in the overall c.m. system and \vec{p} the momentum in the rest frame of the ${}^3\text{He} - n$ subsystem. The following variables were constructed accordingly: $\cos\theta_q$, $\cos\theta_p$ (the polar angles of \vec{q} and \vec{p} , respectively), $M_{3\text{He}n}$ and φ (the angle between the projections of \vec{q} and \vec{p} onto the xy-plane). As discussed earlier all plots show data after a symmetrization in the global c.m. system.

The absolute normalization was done relative to the $dd \rightarrow {}^3\text{He}n$ reaction. Corresponding data were taken in parallel during the first part of the run using a dedicated trigger. Due to the correlation between kinetic energy and scattering angle for the binary reaction, quasi mono-energetic particles form a distinct and clean peak in the $\Delta E - \Delta E$ plots. For the selected events the ${}^3\text{He}$ missing mass distribution reveals a background free peak at the mass of the neutron (Fig. 2a). In order to determine the integrated luminosity the data presented in Ref. [17] were used. The authors measured the reaction $dd \rightarrow {}^3\text{He}p$ for beam momenta between 1.09 GeV/c - 1.78 GeV/c and $dd \rightarrow {}^3\text{He}n$ for beam momenta in the range of 1.65 GeV/c - 2.5 GeV/c. Moreover, they showed that the differential cross sections for both channels at 1.65 GeV/c are identical within the presented errors. Based on these results we used the measured cross sections for $dd \rightarrow {}^3\text{He}p$ to

calculate the cross sections for $dd \rightarrow {}^3\text{He}n$ at 1.2 GeV/c. For this the angular distributions for the beam momenta of 1.109 GeV/c, 1.387 GeV/c and 1.493 GeV/c were parametrized. Then, for selected polar angles the dependence of the differential cross section on the beam momentum was fitted and interpolated to the beam momentum of 1.2 GeV/c. The resulting distribution was used as an input for the simulation of $dd \rightarrow {}^3\text{He}n$. Figure 2b shows the match of the angular distribution of ${}^3\text{He}$ in data and the Monte-Carlo filtered event generator. The extracted integrated luminosity is determined to be $L_{int}^1 = (877 \pm 2_{stat} \pm 62_{sys} \pm 62_{norm}) \text{ nb}^{-1}$, where the superscript 1 refers to the first part of the run. The systematic uncertainty reflects different parametrizations of the reference cross sections. In addition, the uncertainty of 7% in the absolute normalization of the reference data is also included. The result for the total cross section given below is based only on this first part of the run. The second part was optimized for high luminosities and also served as a pilot run for a measurement of $dd \rightarrow {}^4\text{He}\pi^0$. It provided data to extract high statistics differential distributions for $dd \rightarrow {}^3\text{He}n\pi^0$. These have been absolutely normalized relative to the first part of the run using the rates of the $dd \rightarrow {}^3\text{He}n\pi^0$ reaction. The integrated luminosity obtained for the second part of the run amounts to $L_{int}^2 = (4909 \pm 13_{stat} \pm 350_{sys} \pm 350_{norm}) \text{ nb}^{-1}$.

The uncertainty on the integrated luminosity (in total 10% if all contributions are added quadratically) is the dominant source for the systematic error on the absolute normalization. Another source is associated with the cut on the cumulated probability distribution of the kinematic fit. In order to quantify the influence of this cut, the analysis was repeated for different regions in the probability distribution. For the total cross section the maximum deviation from the average value was taken as error. Changes in the shape of the differential distributions were extracted similarly, however excluding the variation in the absolute scale. For all other analysis conditions according to the criteria discussed in Ref. [18] no significant systematic effect was observed.

PHENOMENOLOGICAL MODELS

Presently, no theoretical calculation exists for a microscopic description of the investigated reaction. However, in order to have a sufficiently precise acceptance correction a model which reproduces the experimental data reasonably well is required. The ansatz used here is the incoherent sum of a quasi-free reaction mechanism based on $dp \rightarrow {}^3\text{He}\pi^0$ and a partial-wave expansion for the 3-body reaction. While the latter is limited to s - and p -waves, the large relative momenta between the spectator nucleon and the rest system in the quasi-free model corresponding to higher partial waves motivate the incoherent sum and the neglect of interference terms.

Quasi-free reaction model

High momentum transfer reactions involving a deuteron can proceed via the interaction with a single nucleon of the deuteron and with the second nucleon being regarded as a spectator. Naturally, this mechanism is most significant in regions of the phase space where the momentum of one nucleon in final state matches the typical Fermi momenta in the deuteron. In the present experiment two deuterons are involved and, thus, the reaction may proceed with a projectile or target neutron spectator. For the parametrization of the quasi-free sub reaction $dp \rightarrow {}^3\text{He}\pi^0$, the empirical angular distributions and the energy dependent cross section in the energy regime from threshold up to an excess energy of 10 MeV [19] and for excess energies of 40, 60 and 80 MeV [20] have been used. They have been convoluted with the momentum distribution of the proton in the

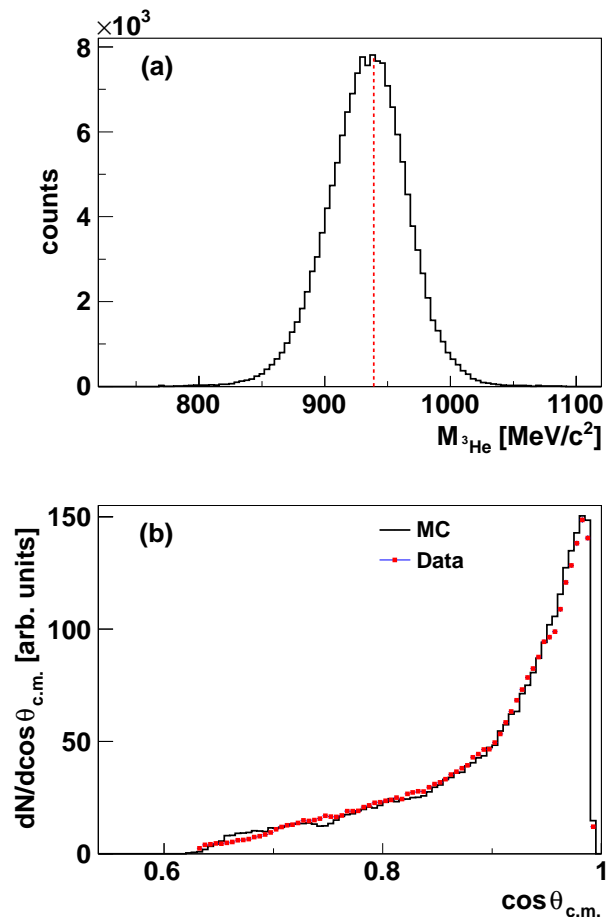


FIG. 2. (Color online) Measurement of the $dd \rightarrow {}^3\text{He}n$ reaction. (a) ${}^3\text{He}$ missing mass distribution, the vertical red dotted line indicates the neutron mass. (b) Measured angular distribution in comparison with a Monte Carlo simulation based on a parametrized cross section (see text).

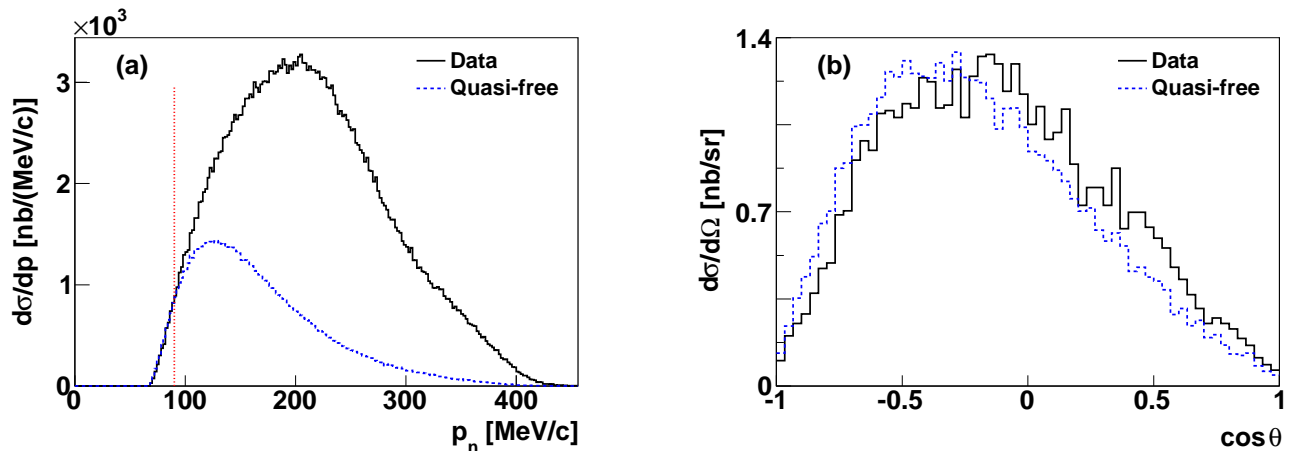


FIG. 3. (Color online) Comparison of data (black line) and the quasi-free model filtered by Monte-Carlo (blue dotted curve). (a) Momentum distribution of the neutron. (b) Angular distribution of the pion in the ${}^3\text{He}-\pi^0$ subsystem for neutron momenta smaller than 90 MeV/c (indicated by the vertical red dotted line in the upper plot). Data are not corrected for acceptance.

deuteron using an analytical form of the deuteron wave function based on the Paris potential [21]. As a result one gets absolutely normalized differential cross sections for the quasi-free contribution to $dd \rightarrow {}^3\text{He}n\pi^0$, which can be directly compared to the measured data. Figure 3a shows the momentum distribution of the neutron for data and the quasi-free model filtered by Monte-Carlo. As expected the quasi-free process dominates the distribution for small momenta. The lower boundary of the spectrum is caused by kinematic effects. At a beam momentum of 1.2 GeV/c the reaction $dp \rightarrow {}^3\text{He}n\pi^0$ with the target proton at rest is below threshold and can only occur for $p_{\text{fermi}} > 48$ MeV/c. The vanishing acceptance at $\theta_{3\text{He}} < 3^\circ$ further increases the minimum Fermi momentum. Figure 3b shows the angular distribution of the pion in the ${}^3\text{He}-\pi^0$ subsystem for neutron momenta below 90 MeV/c, *i.e.* in the region where the quasi-free process should dominate the distribution.

Partial wave decomposition

For the remaining part of the data which cannot be described with the quasi-free process a 3-body model based on a partial wave decomposition has been developed. The relative angular momenta were defined according to the coordinates introduced earlier: one in the global $\pi^0 - ({}^3\text{He}n)$ system and one in the ${}^3\text{He} - n$ subsystem (denoted by l and L , respectively). For the partial wave decomposition the angular momenta have been limited to $l + L \leq 1$, *i.e.* to at most one p -wave in the system. For the momentum dependence the standard approximation $|M|^2 \propto q^{2l}p^{2L}$ was used. Taking into account all possible spin configurations this results in 18 possible amplitudes. After combining the amplitudes with the same signature in final state, four possible contributions can be identified: s -wave in both systems (sS), one p -wave in either system (sP and pS) and a $sP - pS$ interference term. They can be described by seven real coefficients (four complex amplitudes minus one overall phase). With this the four-fold differential cross section can be written as:

$$\frac{d^4\sigma}{2\pi dM_{3\text{He}n} d\cos\theta_p d\cos\theta_q d\varphi} = Cpq \left[A_0 + A_1q^2 + A_3p^2 + \frac{1}{4}A_2q^2(1 + 3\cos 2\theta_q) + \frac{1}{4}A_4p^2(1 + 3\cos 2\theta_p) + A_5pq \cos\theta_p \cos\theta_q + A_6pq \sin\theta_p \sin\theta_q \cos\varphi \right] \quad (1)$$

with

$$C = \frac{1}{32(2\pi)^5 sp_a^*(2s_a + 1)(2s_b + 1)} \quad (2)$$

where s_a and s_b denote the spin of beam and target and s and p_a^* the total energy squared and the beam momen-

tum, respectively, in the c.m. system. The coefficients A_i describe the strength of the individual contributions mentioned above: A_0 corresponds to $l = L = 0$ (sS), A_1 and A_2 to $l = 1$ and $L = 0$ (pS), A_3 and A_4 to $l = 0$ and $L = 1$ (sP) and A_5 and A_6 to the interference term.

Integration of Eq. 1 results in a set of equations for the description of the single differential cross sections:

$$\frac{d\sigma}{dM_{3\text{Hen}}} = 16\pi^2 C p q [A_0 + A_1 q^2 + A_3 p^2] \quad (3a)$$

$$\frac{d\sigma}{2\pi d \cos \theta_q} = 4\pi C \left[B + \frac{1}{4} A_2 (1 + 3 \cos 2\theta_q) I_{pS} \right] \quad (3b)$$

$$\frac{d\sigma}{2\pi d \cos \theta_p} = 4\pi C \left[B + \frac{1}{4} A_4 (1 + 3 \cos 2\theta_p) I_{sP} \right] \quad (3c)$$

$$\frac{d\sigma}{d\varphi} = 8\pi C \left[B + \frac{\pi^2}{16} A_6 I_{pS+sP} \cos \varphi \right] \quad (3d)$$

with the new coefficient

$$B = A_0 I_{sS} + A_1 I_{pS} + A_3 I_{sP}. \quad (4)$$

The constants I_{sS} , I_{pS} , I_{sP} and I_{pS+sP} are the results of the integration over $M_{3\text{Hen}}$:

$$I_{sS} = \int_{(M_{3\text{He}}+M_n)^2}^{(\sqrt{s}-M_\pi)^2} p q dM_{3\text{Hen}} \quad (5a)$$

$$I_{pS} = \int_{(M_{3\text{He}}+M_n)^2}^{(\sqrt{s}-M_\pi)^2} p q^3 dM_{3\text{Hen}} \quad (5b)$$

$$I_{sP} = \int_{(M_{3\text{He}}+M_n)^2}^{(\sqrt{s}-M_\pi)^2} p^3 q dM_{3\text{Hen}} \quad (5c)$$

$$I_{pS+sP} = \int_{(M_{3\text{He}}+M_n)^2}^{(\sqrt{s}-M_\pi)^2} p^2 q^2 dM_{3\text{Hen}} \quad (5d)$$

Equations 3 do not contain the coefficient A_5 as the corresponding term vanishes with the integration over $\cos \theta_q$ and $\cos \theta_p$. In order to extract this coefficient Eq. 1 has to be multiplied by $\cos \theta_q \cos \theta_p$ before integration. This results in the following formula to determine A_5 :

$$\frac{d\sigma'}{d\varphi} = \frac{8}{9} \pi C A_5 I_{pS+sP} \quad (6)$$

with $\sigma'(q, p) = \sigma(q, p) \cdot \cos \theta_q \cos \theta_p$.

It has to be noted that the coefficients A_0 , A_1 and A_3 cannot be extracted unambiguously from the differential distribution $d\sigma/dM_{3\text{Hen}}$. In the non-relativistic limit q^2 and p^2 are both linear in $M_{3\text{Hen}}$ introducing a correlation of all three coefficients. For the measurement of $dd \rightarrow {}^3\text{He}n\pi^0$ at an excess energy of $Q \approx 40$ MeV a non-relativistic treatment is still a good approximation. Thus, only a value for B can be extracted from the data. Any values for A_0 , A_1 and A_3 fulfilling Eq. 4 and the fit to $d\sigma/dM_{3\text{Hen}}$ will lead to the same model description. However, in order to provide a complete set of coefficients the parameter A_1 has been fixed manually.

RESULTS

In a first step a sum of Monte-Carlo filtered distributions for each contribution from the partial wave decomposition (coefficients A_0 to A_6) and from the quasi-free

model (coefficient A_7) was fitted to the uncorrected, single differential spectra. The result served as input for the Monte-Carlo simulation finally used to determine the acceptance correction.

The final distributions after acceptance correction are presented in Fig. 4. Contributions from the quasi-free model, the partial wave decomposition and the full model are shown in blue, green and red, respectively. These spectra were refitted using the analytical formulas given in the previous section. The result is consistent with the initial fit. Although the partial wave expansion was limited to at most one p -wave in the final state it provides a reasonable overall description of the data: both angular distributions show a significant contribution of p -waves of similar size, the pS - sP interference term is visualized by the non-isotropic distribution of $d\sigma/d\varphi$. The quasi-free contribution is about $1.11 \mu\text{b}$ and, thus, is in agreement with the prediction of the quasi-free model ($1.19 \mu\text{b}$) within the normalization error of about 10% given in Ref. [19]. The result of the fit using Eq. 6 and the quasi-free model is presented in Fig. 5. The values for the extracted coefficients from the global fit are summarized in Table I.

One should emphasize that the meaning of the fit parameters is limited to the context of the discussed model. Any addition of higher partial waves, for example, would also change the extracted amplitudes of the lower partial waves. Thus, systematic errors are only provided for data. For the extracted fit parameters only statistical errors are given.

So far, a possible momentum dependence of the transition amplitudes, for example due to initial or final state interaction, was neglected. Deviations from this assumption were studied by refitting the data for five intervals in $M_{3\text{Hen}}$ (corresponding to intervals in \vec{q} and \vec{p}). All coefficients except one remained constant. Only A_4 representing a p -wave contribution in the ${}^3\text{He}n$ system showed a significant momentum dependence (see Fig. 6): A_4 is

Parameter	Fit result
B	(1.840 \pm 0.003) μb
A_0	(0.41 \pm 0.01) $\cdot 10^4 \mu\text{b}/\text{GeV}^3$
A_1	8.4 $\cdot 10^4 \mu\text{b}/\text{GeV}^5$
A_2	(18.3 \pm 0.3) $\cdot 10^4 \mu\text{b}/\text{GeV}^5$
A_3	(1.08 \pm 0.05) $\cdot 10^4 \mu\text{b}/\text{GeV}^5$
A_4	(18.04 \pm 0.07) $\cdot 10^4 \mu\text{b}/\text{GeV}^5$
A_5	(-45.4 \pm 0.3) $\cdot 10^4 \mu\text{b}/\text{GeV}^5$
A_6	(-15.0 \pm 0.2) $\cdot 10^4 \mu\text{b}/\text{GeV}^5$
$\sigma_{qf} \cdot A_7$	(1.108 \pm 0.003) μb

TABLE I. Collection of the extracted fit parameters. The amplitudes are given in units of $(4\pi)^2 C$. The parameters A_0 , A_1 and A_3 are correlated and could not be extracted unambiguously: the given numbers represent one possible solution with A_1 being fixed (see text).

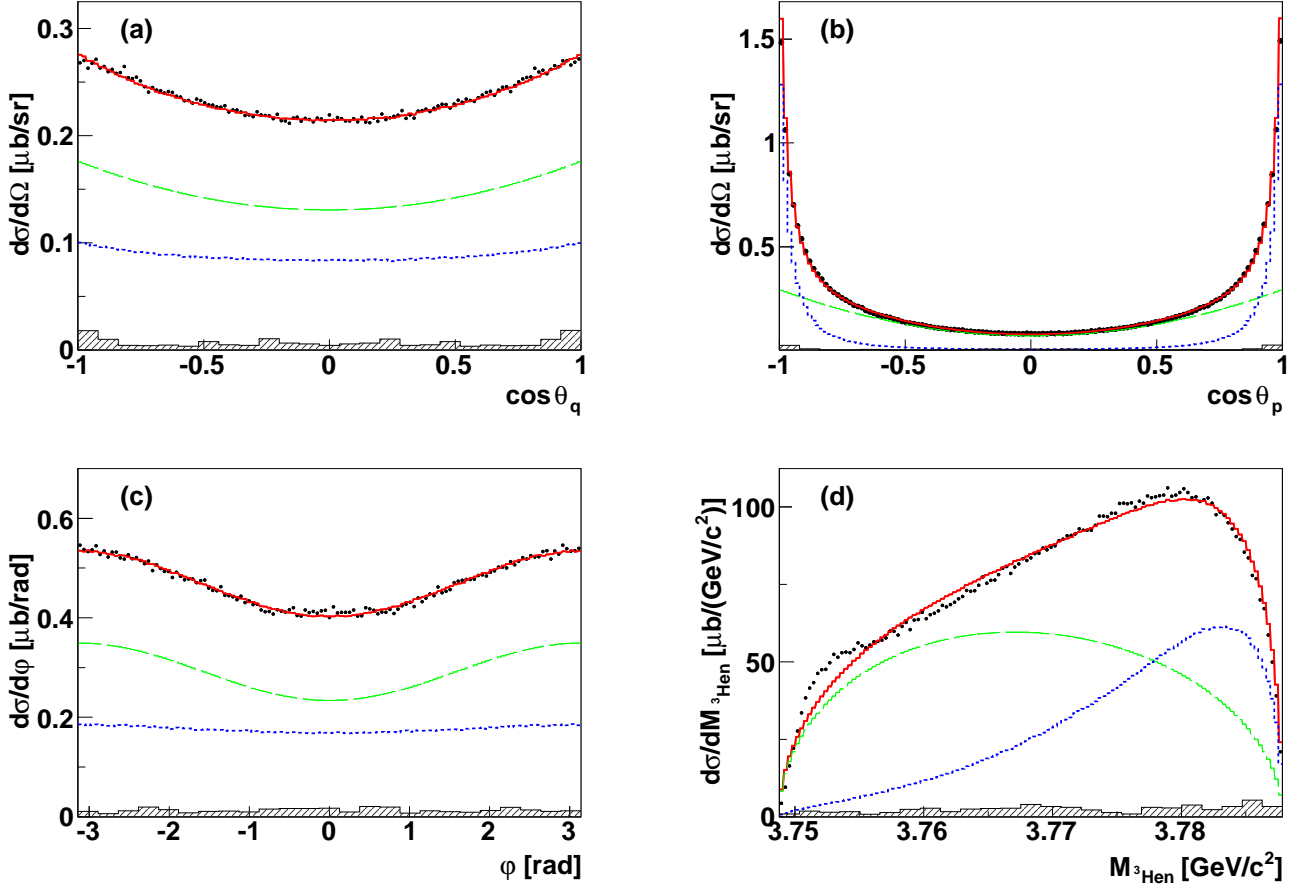


FIG. 4. (Color online) Acceptance corrected data (black points) presented as functions of (a) $\cos \theta_q$, (b) $\cos \theta_p$, (c) φ and (d) $M_{3\text{He}-n}^2$. The curves represent the fit to the model: full model (red solid), quasi-free contribution (blue dotted) and the partial wave decomposition (green long dashed). The hatched areas indicate the systematic uncertainties on the shape of the differential distributions. Uncertainties on the absolute normalization are not included.

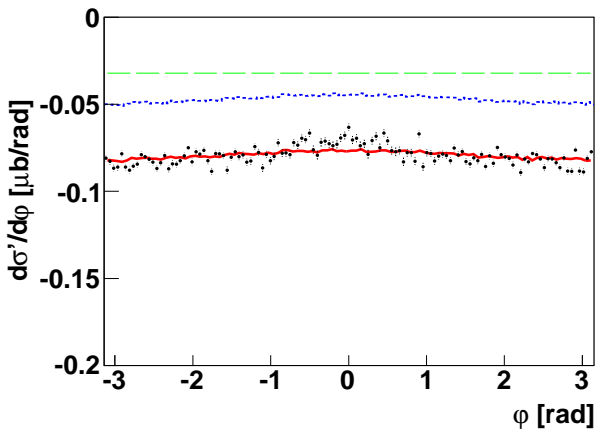


FIG. 5. (Color online) Distribution of $d\sigma'/d\varphi$ as used in Eq. 6 to extract A_5 . For the definition of the curves see Fig. 4.

larger for low excess energies in the ${}^3\text{He}-n$ system (corresponding to low relative momenta). One possible reason for this might be excited states with isospin $I = 1$ in the ${}^3\text{He}-n$ system at low excess energies as reported in Ref. [22] (the production of an $I = 0$ state would be charge symmetry breaking).

Figure 7 shows the acceptance corrected Dalitz plot for $M_{n\pi}^2$ versus $M_{3\text{He}-n}^2$. It should be noted that the Dalitz plot is fully covered except for a small region for large $\pi^0 - n$ invariant masses due to the acceptance hole for $\theta_{3\text{He}} < 3^\circ$. The quasi-free reaction process mainly populates the region for small $\pi^0 - n$ invariant masses and large ${}^3\text{He} - n$ invariant masses. The observation of an increasing p -wave contribution for small excess energies in the ${}^3\text{He}-n$ system possibly caused by an excited $I = 0$ state comes with an enhancement in the Dalitz plot for small ${}^3\text{He} - n$ invariant masses.

Integrating over the differential distributions we obtain

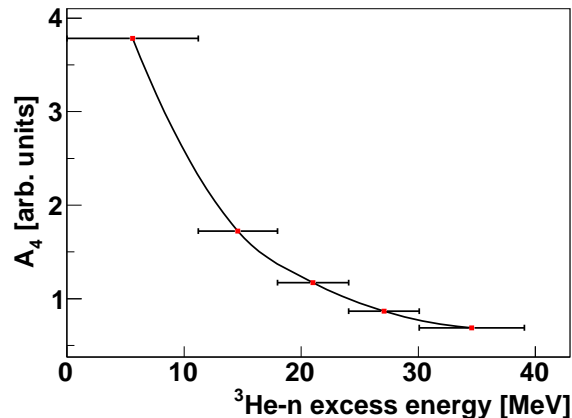


FIG. 6. Coefficient A_4 in the ${}^3\text{He} - n$ system as a function of the excess energy: the strength of the p -wave contribution increases for small excess energies. The error bars along the x -axis represent the width of the intervals in $M_{3\text{He}n}$.

for the total cross section of the $dd \rightarrow {}^3\text{He}n\pi^0$ reaction:

$$\sigma_{tot} = (2.89 \pm 0.01_{stat} \pm 0.06_{sys} \pm 0.29_{norm}) \mu\text{b}. \quad (7)$$

SUMMARY

For the first time an exclusive measurement of the $dd \rightarrow {}^3\text{He}n\pi^0$ reaction has been performed. A total cross section of $\sigma_{tot} = 2.89 \mu\text{b}$ with an accuracy of about 11% has been extracted. Differential distributions have been compared to the incoherent sum of a quasi-free reaction model and a partial-wave expansion limited to at most one p -wave in the final state. The contribution of the quasi-free processes accounts for about $1.11 \mu\text{b}$ of the total cross section matching the prediction of the quasi-free reaction model. The partial wave decomposition reveals the importance of p -wave contributions in the final state. The applied model shows a reasonable agreement for all differential distribution. Thus, based on this comparison no indication for significant contributions of higher partial waves can be deduced.

The whole data set amounts to about 3.4×10^6 fully reconstructed and background-free events. The presented differential distributions are only one possible representation of the results. One goal of the measurement was to provide data for studying dd initial state interaction for small angular momenta, which is one missing information in the microscopic description of the charge symmetry breaking reaction $dd \rightarrow {}^4\text{He}\pi^0$ within the framework of Chiral Perturbation Theory. Once the important observables have been identified the corresponding experimental distributions can be provided.

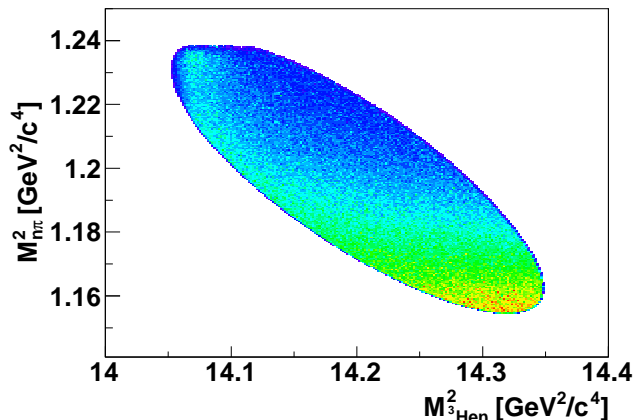


FIG. 7. (Color online) Acceptance corrected Dalitz plot. The region with low values of $M_{n\pi}^2$ and large values of $M_{3\text{He}n}^2$ is dominated by the quasi-free process. The enhancement at low values of $M_{3\text{He}n}^2$ corresponds to the low mass enhancement in Fig. 4d and might be connected to the energy dependence of the p -wave amplitude discussed in Fig 6. At large values of $M_{n\pi}^2$ the Dalitz plot is cut due to the acceptance hole for $\theta_{3\text{He}} < 3^\circ$.

ACKNOWLEDGMENTS

We would like to thank the technical and administrative staff at the Forschungszentrum Jülich, especially at the COoler SYNchrotron COSY and at the participating institutes. This work has been supported in part by the German Federal Ministry of Education and Research (BMBF), the Polish Ministry of Science and Higher Education, the Polish National Science Center (grant No. 2011/01/B/ST2/00431), the Foundation for Polish Science (MPD), Forschungszentrum Jülich (COSY-FFE) and the European Union Seventh Framework Programme (FP7/2007-2013) under grant agreement No. 283286.

* Electronic address: v.hejny@fz-juelich.de

† Present address: Department of Physics and Astrophysics, University of Delhi, Delhi-110007, India

‡ Present address: Department of Physics, Stockholm University, Roslagstullsbacken 21, AlbaNova, 10691 Stockholm, Sweden

§ Present address: Institut für Kernphysik, Johannes Gutenberg-Universität Mainz, Johann-Joachim-Becher Weg 45, 55128 Mainz, Germany

¶ Present address: Department of Physics and Astronomy, University of California, Los Angeles, California-90045, U.S.A.

** Present address: Albert Einstein Center for Fundamental Physics, Fachbereich Physik und Astronomie, Universität Bern, Sidlerstr. 5, 3012 Bern, Switzerland

[1] S. Weinberg, Trans. N.Y. Acad. Sci. **38**, 185 (1977).

- [2] J. Gasser and H. Leutwyler, Phys. Rep. **87**, 77 (1982).
- [3] H. Leutwyler, Phys. Lett. **B378**, 133 (1996).
- [4] G. Miller *et al.*, Phys. Rep. **194**, 1 (1990).
- [5] N. Fettes, U.-G. Meißner and S. Steininger, Phys. Lett. **B451**, 233 (1999); M. Hoferichter, B. Kubis and U.-G. Meißner, Phys. Lett. **B678**, 65 (2009).
- [6] E. Stephenson *et al.*, Phys. Rev. Lett. **91**, 142302 (2003).
- [7] A. Opper *et al.*, Phys. Rev. Lett. **91**, 212302 (2003).
- [8] G.A. Miller *et al.*, Ann. Rev. Nucl. Part. Sci. **56**, 253 (2006).
- [9] A. Filin *et al.*, Phys. Lett. **B681**, 423 (2009).
- [10] C. Hanhart *et al.*, Phys. Rep. **397**, 155 (2004).
- [11] A. Gårdestig *et al.*, Phys. Rev. C **69**, 044606 (2004).
- [12] A. Nogga *et al.*, Phys. Lett. **B639**, 465 (2006).
- [13] T. A. Lähde and G. A. Miller, Phys. Rev. C **75**, 055204 (2007)
- [14] A. C. Fonseca, R. Machleidt and G. A. Miller, Phys. Rev. C **80**, 027001 (2009).
- [15] R. Maier *et al.*, Nucl. Phys. **A626**, 395c (1997).
- [16] H. H. Adam *et al.* (WASA-at-COSY Collaboration), arXiv:nucl-ex/0411038 (2004).
- [17] G. Bizard *et al.*, Phys. Rev. C **22**, 1632 (1980).
- [18] R. Barlow, arXiv:hep-ex/0207026 (2002).
- [19] V. N. Nikulin *et al.*, Phys. Rev. C **54**, 1732 (1996).
- [20] M. Betigeri *et al.*, Nucl. Phys. **A690**, 473 (2001).
- [21] M. Lacombe *et al.*, Phys. Lett. **B101**, 139 (1981).
- [22] D. R. Tilley *et al.*, Nucl. Phys. **A541**, 1 (1992).